

Non-Fermi-liquid behaviour of electrons coupled to gauge phonons

Rutvij Gholap,¹ Alexey Ermakov,¹ Alexander Kazantsev,¹ Mohammad Saeed Bahramy,¹ Marco Polini,² and Alessandro Principi¹

¹*School of Physics and Astronomy, University of Manchester*

²*Dipartimento di Fisica dell'Università di Pisa, Largo Bruno Pontecorvo 3, I-56127 Pisa, Italy*

(Dated: March 19, 2026)

We identify overdamped gauge phonons as a new microscopic route to non-Fermi-liquid behaviour in Dirac materials. These phonons couple to electronic currents rather than densities, thereby realising a lattice analogue of transverse gauge-field mechanisms without requiring proximity to a quantum critical point. By computing the electronic self-energy with a phonon propagator dressed by electron-phonon interactions, we show that the low-energy behaviour is controlled by the orbital susceptibility χ and a dimensionless damping parameter $\bar{\alpha}$. In the overdamped regime, $\bar{\alpha} \gg 1$, quasiparticles display strong deviations from Fermi-liquid theory. For $\chi > 0$, Fermi-liquid behaviour persists only in a parametrically narrow infrared window before crossing over to non-Fermi-liquid scaling. For $\chi < 0$, the Fermi-liquid regime is replaced by marginal-Fermi-liquid behaviour at the lowest energies, followed by a crossover to non-Fermi-liquid scaling. These results establish strain-induced gauge phonons as a promising source of anomalous metallic behaviour in systems such as twisted bilayer graphene.

Introduction—Landau's Fermi-liquid (FL) theory provides the canonical low-energy description of interacting metals in terms of long-lived fermionic quasiparticles [1–3]. In this picture, the phase space available for scattering is strongly restricted near the Fermi surface, so that at zero temperature the quasiparticle decay rate scales as $\Gamma \propto \varepsilon^2$, vanishing faster than the excitation energy ε . As a result, interactions renormalize quasiparticle properties, such as the effective mass and response functions, but preserve the basic quasiparticle description and the overall low-energy phenomenology of the metal. However, many correlated metals exhibit robust non-Fermi-liquid (NFL) behaviour. In particular, an electrical resistivity that is approximately linear in temperature over broad parameter ranges is widely regarded as a hallmark of strange-metal phenomenology [4, 5]. These observations motivate the search for generic microscopic mechanisms that can produce deviations from Fermi-liquid behaviour down to the lowest energies.

One standard route to the breakdown of Landau's Fermi-liquid picture is the coupling of electrons to gapless bosonic collective fluctuations. A weak departure from Fermi-liquid behaviour occurs in the marginal-Fermi-liquid (MFL) scenario, in which the quasiparticle decay rate scales linearly with energy, $\Gamma \propto \varepsilon$, and is therefore not parametrically smaller than the quasiparticle energy [6].

A more pronounced breakdown of the quasiparticle picture occurs in quantum-critical metals, which provide a canonical setting for NFL behaviour. For example, within the Hertz–Millis framework [7, 8], coupling to overdamped order-parameter fluctuations can strongly renormalize the low-energy fermionic self-energy. In two dimensions, this coupling can, in certain cases, produce a quasiparticle decay rate $\Gamma(\varepsilon) \propto \varepsilon^{2/3}$, which becomes parametrically larger than the excitation energy as $\varepsilon \rightarrow 0$, signaling the breakdown of the quasiparticle description. Other power laws may arise depending on

the universality class and on the structure of the critical fluctuations [9–12].

Recent work has also highlighted spatial randomness as an additional ingredient in strange-metal phenomenology. In particular, in two-dimensional quantum-critical metals, random Yukawa couplings were shown to generate robust T -linear resistivity together with other universal strange-metal signatures [13].

A further broad class of NFL states arises when fermions couple to overdamped transverse gauge fluctuations. Unlike quantum-critical scenarios, this mechanism does not require proximity to a continuous phase transition. In two dimensions, such an interaction can result in a fermion decay rate $\Gamma(\varepsilon) \propto \varepsilon^{2/3}$, signaling the breakdown of the quasiparticle description [14–17]. Microscopically, the gauge field couples to the electronic current. The resulting low-energy interaction is therefore renormalized by the dynamical transverse current-current response, whose long-wavelength form includes both a regular q^2 contribution (proportional to the orbital magnetic susceptibility χ) and a Landau-damping term, controlled by a dimensionless parameter $\bar{\alpha}$. When $\bar{\alpha} \gg 1$, gauge fluctuations are overdamped and NFL behaviour emerges. A realization of this mechanism has recently been proposed in strongly coupled cavity QED near the onset of a superradiant transition [18, 19]. This suggests that any bosonic mode coupling predominantly to electronic currents, rather than densities, may provide an alternative route to NFL behaviour.

In this work, we show that *gauge phonons* [20], which couple to electronic currents rather than densities, can induce pronounced NFL behaviour. Such couplings arise naturally in crystals with non-orthogonal lattice vectors. In two dimensions, relevant examples include oblique and triangular lattices, as well as strained square or rectangular structures [21]. Motivated by the broad relevance of this mechanism, we focus here on experimentally accessible Dirac materials, in particular magic-angle twisted

bilayer graphene (MATBG), where lattice deformations act as effective valley-dependent gauge fields [22, 23].

We show this by computing the electronic self-energy at leading nontrivial order, with the transverse phonon propagator dressed by the electron-phonon interaction. When gauge phonons become strongly damped, they provide a new route to NFL behaviour, distinct from conventional order-parameter criticality and closely related to mechanisms based on transverse gauge fluctuations.

The resulting low-energy physics is controlled by the orbital response χ and the damping parameter $\bar{\alpha}$. NFL behaviour develops for $\bar{\alpha} \gg 1$. We distinguish two cases. For $\chi > 0$, the electronic self-energy exhibits a quantum-critical-like crossover structure. Although the system remains Fermi-liquid-like within an extremely narrow low-energy window, much narrower than in conventional Fermi liquids, it rapidly crosses over to an NFL regime. By contrast, for $\chi < 0$, the softening of the gauge-phonon dispersion replaces the Fermi-liquid infrared behaviour by a marginal-Fermi-liquid one, which in turn crosses over to stronger NFL scaling at higher energies.

Model—We consider a generic non-interacting electron Hamiltonian, $\mathcal{H}_e = \sum_{\mathbf{k}, \lambda} \xi_{\mathbf{k}, \lambda} c_{\mathbf{k}, \lambda}^\dagger c_{\mathbf{k}, \lambda}$, where λ is the band index, $\xi_{\mathbf{k}, \lambda} = \varepsilon_{\mathbf{k}, \lambda} - \mu$, $\varepsilon_{\mathbf{k}, \lambda}$ is the band energy, and μ is the chemical potential. We focus on graphene in the Dirac limit, $\varepsilon_{\mathbf{k}, \lambda} = \lambda v_F k$, with $\lambda = +1$ ($\lambda = -1$) labelling the conduction (valence) band (hereafter, $\hbar = 1$). Here v_F is the Fermi velocity of graphene electrons near the K and K' points of the Brillouin zone.

The bare phonon Hamiltonian is $\mathcal{H}_{\text{ph}} = \sum_{\mathbf{q}, \nu} \omega_{\mathbf{q}, \nu} a_{\mathbf{q}, \nu}^\dagger a_{\mathbf{q}, \nu}$, where $\omega_{\mathbf{q}, \nu} = c_{\text{ph}, \nu} q$ is the acoustic phonon dispersion, $c_{\text{ph}, \nu}$ is the sound velocity, and $\nu = \text{L, T}$ distinguishes longitudinal and transverse modes. For graphene we use $c_{\text{ph}, \text{L}} = 2.2 \times 10^6$ cm/s and $c_{\text{ph}, \text{T}} = 1.4 \times 10^6$ cm/s [20, 24]. Lattice distortions modify the electronic hopping amplitudes and generate both scalar and vector electron-phonon couplings. The corresponding low-energy Hamiltonian can be written as

$$\mathcal{H}_{\text{e-ph}} = \sum_{\mathbf{k}, \mathbf{q}, \alpha, \beta} c_{\mathbf{k}-\mathbf{q}, \alpha}^\dagger \left(\mathbf{A}_{\mathbf{q}} \cdot \mathbf{j}_{\mathbf{q}} + V_{\mathbf{q}} \mathbb{1} \right)_{\alpha\beta} c_{\mathbf{k}, \beta}, \quad (1)$$

where $V_{\mathbf{q}}$ is the scalar deformation-potential coupling and $\mathbf{A}_{\mathbf{q}}$ is the strain-induced gauge field, whose longitudinal and transverse components mix phonon polarizations. Since the scalar coupling is screened whereas the gauge coupling is not, the low-energy self-energy studied below is controlled by the latter. Further details of $\mathcal{H}_{\text{e-ph}}$ and the associated couplings are given in appendix A.

Self-energy.— We consider the one-loop electron-phonon self-energy $\Sigma_\lambda(\mathbf{k}, i\varepsilon_n)$ to second order in perturbation theory shown in Fig. 1. The self-energy reads,

$$\Sigma_\lambda(\mathbf{k}, i\varepsilon_n) = -\beta^{-1} \sum_{\omega_m} \sum_{\nu, \nu', \lambda'} \int \frac{d^2 \mathbf{q}}{(2\pi)^2} D^{\nu, \nu'}(\mathbf{q}, i\omega_m) \times G_{\lambda'}^{(0)}(\mathbf{k} + \mathbf{q}, i\varepsilon_n + i\omega_m) j_{\mathbf{k}, \lambda; \mathbf{k} + \mathbf{q}, \lambda'}^\nu j_{\mathbf{k} + \mathbf{q}, \lambda'; \mathbf{k}, \lambda}^{\nu'}. \quad (2)$$

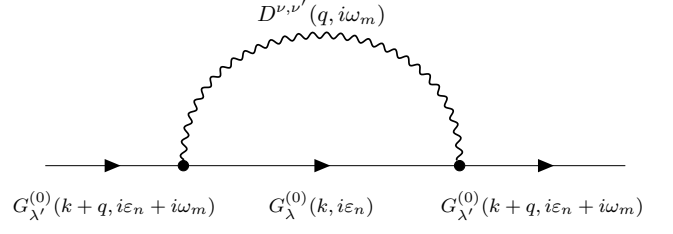


FIG. 1. One-loop electron-phonon contribution to the self-energy $\Sigma_\lambda(\mathbf{k}, i\varepsilon_n)$.

Here $\varepsilon_n = (2n + 1)\pi/\beta$ and $\omega_m = 2m\pi/\beta$ are fermionic and bosonic Matsubara frequencies, respectively, $D^{\nu, \nu'}(\mathbf{q}, i\omega_m)$ is the dressed phonon propagator, and $G_{\lambda}^{(0)}(\mathbf{k}, i\varepsilon_n) = 1/(i\varepsilon_n - \xi_{\mathbf{k}, \lambda})$ is the bare electron Green's function.

After analytic continuation $i\varepsilon_n \rightarrow \varepsilon + i0^+$, the imaginary part of the retarded self-energy can be written as

$$\Im m \Sigma_\lambda^{(R)}(\mathbf{k}, \varepsilon) = - \int_{-\infty}^{\infty} \frac{d\omega}{\pi} [n_B(\omega) + n_F(\omega + \varepsilon)] \times \sum_{\nu, \nu', \lambda'} \int \frac{d^2 \mathbf{q}}{(2\pi)^2} \Im m D^{\nu, \nu'}(\mathbf{q}, \omega) \Im m G_{\lambda'}^{(0)}(\mathbf{k} + \mathbf{q}, \varepsilon + \omega) \times j_{\mathbf{k}, \lambda; \mathbf{k} + \mathbf{q}, \lambda'}^\nu j_{\mathbf{k} + \mathbf{q}, \lambda'; \mathbf{k}, \lambda}^{\nu'}. \quad (3)$$

We now focus on the low-energy self-energy at the Fermi surface. For $\mathbf{k} \simeq \mathbf{k}_F$ and $T \rightarrow 0$, the chemical potential coincides with the Fermi energy of the non-interacting system, $\mu = \varepsilon_F = v_F k_F$. In this limit the factor $n_B(\omega) + n_F(\omega + \varepsilon)$ restricts the frequency transfer to an interval of width $|\varepsilon|$, while the intermediate fermionic state is pinned close to the Fermi surface. The current matrix elements therefore simplify to

$$j_{\mathbf{k}, \lambda; \mathbf{k}', \lambda'}^{\text{L}} = v_F \frac{i(\lambda' - \lambda)}{2} e^{i(\varphi_{\mathbf{k}'} - \varphi_{\mathbf{k}})/2}, \quad (4)$$

$$j_{\mathbf{k}, \lambda; \mathbf{k}', \lambda'}^{\text{T}} = v_F \frac{\lambda' + \lambda}{2} e^{i(\varphi_{\mathbf{k}'} - \varphi_{\mathbf{k}})/2}. \quad (5)$$

Since at the Fermi surface $\lambda' = \lambda$, the longitudinal matrix element vanishes and only the transverse channel contributes. This is the channel that enters the dressed transverse phonon propagator discussed below. The intermediate steps of the analytic continuation and the Fermi-surface reduction are given in Appendix B.

Dressed phonon propagator.— We focus on the transverse-transverse (TT) propagator that enters the low-energy self-energy at the Fermi surface. Since the transverse gauge field is a linear combination of phonon coordinates (L and T), the bare TT propagator reads,

$$D^{(0), TT}(\mathbf{q}, \omega) = \sum_{\nu=\text{L, T}} g_\nu^2(q) \times [\tilde{M}_{\text{T}, \nu}(\hat{\mathbf{q}})]^2 \frac{2\omega_{\mathbf{q}, \nu}}{(\omega + i0^+)^2 - \omega_{\mathbf{q}, \nu}^2}. \quad (6)$$

where $g_\nu(q) = (g_2/v_F) \times \sqrt{q^2/2\rho_m\bar{\omega}_{q,\nu}}$. For the purpose of scaling analysis, we approximate the longitudinal and transverse acoustic branches by a single effective mode, $\omega_{q,L} \simeq \omega_{q,T} \equiv \bar{\omega}_q$. This simplification only affects overall prefactors and does not modify the scaling exponents discussed below.

We now dress the phonon propagator by electron–hole excitations using an RPA-like resummation. Since the electron–phonon interaction in Eq. (1) couples the gauge field to the electronic current, the polarization entering the Dyson equation is the transverse current–current response. The dressed propagator therefore satisfies

$$[D^{TT}(\mathbf{q}, \omega)]^{-1} = [D^{(0),TT}(\mathbf{q}, \omega)]^{-1} - \chi^{(T)}(\mathbf{q}, \omega). \quad (7)$$

For a non-interacting electron liquid and in the regime $\omega \ll v_F q \ll \varepsilon_F$, the transverse current–current response admits the low-energy expansion

$$\chi^{(T)}(q, \omega) \simeq \chi q^2 - i\alpha \frac{\omega}{v_F q}. \quad (8)$$

The coefficient of the imaginary term, α , describes Landau damping due to particle–hole excitations, while the real coefficient χ determines the stiffness of the transverse response. On dimensional grounds, one has $\alpha \sim \nu_0 v_F^2$ and $\chi \sim \nu_0 v_F^2/k_F^2$, where ν_0 is the density of states at the Fermi energy. We also note that the orbital magnetic susceptibility is proportional to $-\chi$.

Using Eq. (8), the dressed TT phonon propagator takes the form

$$D^{TT}(\mathbf{q}, \omega) = g^2(q) \frac{2\bar{\omega}_q}{(\omega + i0^+)^2 - \bar{\omega}_q^2 - \bar{\chi}q^4 + i\bar{\alpha}q\omega}. \quad (9)$$

Here we introduced the effective parameters $\bar{\chi} = (g_2^2\chi)/(v_F^2\rho_m)$ and $\bar{\alpha} = (g_2^2\alpha)/(v_F^3\rho_m)$. The sign of $\bar{\chi}$ determines whether the real part of the phonon dispersion stiffens ($\bar{\chi} > 0$, corresponding to a diamagnetic response) or softens ($\bar{\chi} < 0$, corresponding to a paramagnetic response), while $\bar{\alpha} > 0$ ensures that the poles of the propagator lie in the lower half of the complex-frequency plane.

To analyse the scaling behaviour, it is convenient to express the self-energy in dimensionless form using the Fermi energy $\varepsilon_F = v_F k_F$. To this end, we define $\bar{q} = q/k_F$, $\bar{\omega} = \omega/(v_F k_F)$, $\bar{\varepsilon} = \varepsilon/(v_F k_F)$, and rescale the susceptibility parameters to a dimensionless form such that, $\bar{\chi} \rightarrow \bar{\chi}k_F^2/v_F^2$ and $\bar{\alpha} \rightarrow \bar{\alpha}/v_F$. The self-energy is thus rewritten as,

$$\begin{aligned} \Im m \Sigma_+^R(k_F, \bar{\varepsilon}) &= \int_0^{\bar{\varepsilon}} \frac{d\bar{\omega}}{\pi} \int_{\bar{\varepsilon}+\bar{\omega}}^{2+(\bar{\varepsilon}+\bar{\omega})} \frac{d\bar{q}}{\pi} \\ &\times \frac{\bar{q}|\bar{\varepsilon} + \bar{\omega} + 1|}{\sqrt{(2\bar{q})^2 - [(\bar{\varepsilon} + \bar{\omega} + 1)^2 - (1 + \bar{q}^2)]^2}} \\ &\times \frac{\bar{\alpha}\bar{q}^3\bar{\omega}}{[\bar{\omega}^2 - (c_{\text{ph}}/v_F)^2\bar{q}^2 - \bar{\chi}\bar{q}^4]^2 + (\bar{\alpha}\bar{q}\bar{\omega})^2}. \end{aligned} \quad (10)$$

The intermediate steps leading to Eq. (10) are presented in Appendix C.

Results.— Figure 2 shows the numerical evaluation of Eq. (10) in the regime of strong Landau damping, $\bar{\alpha} \gg 1$. In this regime, the self-energy deviates from the standard Fermi-liquid form, above the characteristic crossover scale

$$\bar{\varepsilon}_* \sim \frac{(c_{\text{ph}}/v_F)^3}{\bar{\alpha}\sqrt{\bar{\chi}}}. \quad (11)$$

For $\bar{\chi} > 0$, the low-energy regime remains Fermi-liquid like, while at higher energies the self-energy crosses over to a regime controlled by the Landau-damped phonon, whose characteristic momentum scales as $q \sim (\bar{\alpha}\omega/\bar{\chi})^{1/3}$. Figures 2(a) and 2(b) show this crossover for different values of $\bar{\chi}$ and $\bar{\alpha}$, which shift the location of $\bar{\varepsilon}_*$ on a log-log scale. The corresponding local logarithmic slope is shown in Figs. 2(d) and 2(e), where we define $\zeta(\bar{\varepsilon}) = d \ln \Im m \Sigma_+^R(k_F, \bar{\varepsilon})/d \ln \bar{\varepsilon}$. At the lowest energies, $\zeta(\bar{\varepsilon}) \rightarrow 2$ is consistent with Fermi-liquid behaviour, whereas above the crossover, it approaches the non-Fermi-liquid value $\zeta(\bar{\varepsilon}) \simeq 2/3$. This is in agreement with the scaling found more generally in theories of fermions coupled to overdamped transverse bosonic modes [11, 12]. A closely related self-energy study was recently reported by Rao and Piazza [18] for electrons coupled to a critical transverse electromagnetic mode. In both problems, the essential ingredient is a transverse boson that becomes Landau damped by the electronic current response, leading to the same $\varepsilon^{2/3}$ self-energy scaling. In the present case, however, the relevant mode is a phonon-generated gauge field, and for $\bar{\chi} > 0$ the q^4 term stiffens the dressed phonon dispersion. Therefore, Figure 2 uniquely shows a crossover from low-energy Fermi-liquid behaviour to the $\varepsilon^{2/3}$ regime above the scale $\bar{\varepsilon}_*$. An analytical estimate for $\bar{\varepsilon}_*$, together with the asymptotic behaviour of the self-energy in the two regimes, is derived in appendix D.

Figures 2(c) and 2(f) show the behaviour for $\bar{\chi} < 0$, corresponding to a paramagnetic current response. In this regime, the q^4 term softens the dressed phonon dispersion, signalling the proximity to an instability of the transverse mode. As a consequence, the self-energy acquires a qualitatively different scaling structure. In contrast to the $\bar{\chi} > 0$ case, where the infrared regime remains Fermi-liquid like, here the infrared behaviour is no longer described by a Fermi liquid. Instead, the local logarithmic slope approaches $\zeta(\bar{\varepsilon}) \simeq 1$, corresponding to $\Im m \Sigma_+^R(\bar{\varepsilon}) \propto \bar{\varepsilon}$, which is the characteristic signature of a marginal Fermi liquid. As proposed in previous works [18, 25], such an instability may be associated with a superradiant phase transition. The same crossover scale $\bar{\varepsilon}_*$ continues to govern the transition between regimes. While the higher-energy behaviour retains the non-Fermi-liquid $\varepsilon^{2/3}$ scaling associated with the Landau-damped mode, the infrared regime is dominated by a shell of softened phonon modes at the characteristic finite momentum $\bar{q}_{\text{shell}} \sim c_{\text{ph}}/(v_F\sqrt{|\bar{\chi}|})$. This is reminiscent of Brazovskii-type soft-mode physics [26], in which the bosonic spectrum softens not at $q = 0$ but on a finite-momentum shell, thereby enhancing the phase

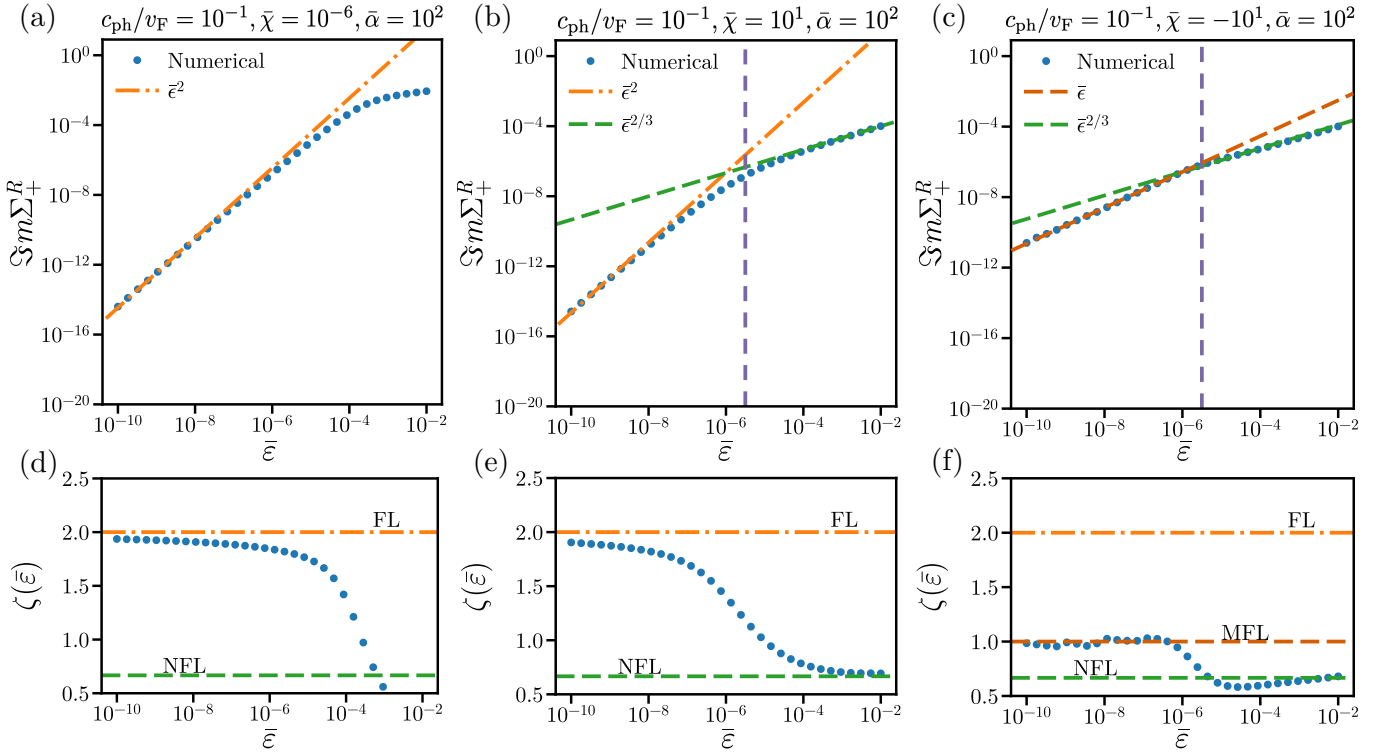


FIG. 2. Imaginary part of the retarded self-energy, $\Im m \Sigma_+^R$, as a function of the dimensionless energy $\bar{\varepsilon}$. The insets show the corresponding local scaling exponent $\zeta(\bar{\varepsilon})$. (a) and (d) correspond to $\bar{\chi} = 10^{-6}, \bar{\alpha} = 10^2$, and $c_{ph}/v_F = 10^{-1}$, and shows predominantly Fermi-liquid like behaviour (as $\bar{\varepsilon}_* = 10^{-2}$). (b) and (e) correspond to $\bar{\chi} = 10^1, \bar{\alpha} = 10^2$, and $c_{ph}/v_F = 10^{-1}$, and show a crossover from Fermi-liquid like scaling toward non-Fermi-liquid behaviour, at $\bar{\varepsilon}_* \simeq 10^{-5}$ (denoted by the purple dashed vertical line), with an effective exponent close to 2/3. (c) and (f) corresponds to $\bar{\chi} = -10^1, \bar{\alpha} = 10^2$, and $c_{ph}/v_F = 10^{-1}$. The crossover from a marginal-Fermi-liquid like regime to a non-Fermi-liquid regime occurs at the same energy, $\bar{\varepsilon}_* \simeq 10^{-5}$.

space of soft fluctuations. In this respect, the $\bar{\chi} < 0$ regime is also analogous to a finite- q instability, as in a charge-density-wave problem, but with the important caveat that the softened modes lie on a shell of momenta rather than at a single ordering wavevector.

The physical content of this regime is distinct from the conventional phenomenological marginal-Fermi-liquid picture. In the original proposal of Varma *et al.* [6], the linear-in-energy scattering rate was introduced phenomenologically in terms of a broad critical bosonic spectrum. Here, by contrast, the marginal-Fermi-liquid scaling emerges microscopically for $\bar{\chi} < 0$. Figures 2(c) and 2(f), together with the analytically derived asymptotic behaviour $\Im m \Sigma_+^R(\bar{\varepsilon}) \propto \bar{\varepsilon}$ in appendix D, show that the present model does not merely reproduce a marginal-Fermi-liquid exponent, but provides a microscopic route to marginal-Fermi-liquid behaviour together with its crossover into the higher-energy non-Fermi-liquid regime, both controlled by the same scale $\bar{\varepsilon}_*$.

We now turn to material estimates for monolayer graphene and magic-angle twisted bilayer graphene (MATBG). To connect the effective theory to experiment, we estimate the parameters entering the dressed transverse phonon propagator in Eq. (9) from the transverse current response. For the static term, we use

the relation [27] $\bar{\chi} = \Re(\chi_{orb})/\mu_0 e^2$, where χ_{orb} is the orbital magnetic susceptibility. Using the value reported in Ref. [27], we take for monolayer graphene, in the near-charge-neutrality regime, where the orbital susceptibility is approximately on a plateau, $\chi = -5.22 \times 10^{29} \text{ m}^2 \text{ J}^{-1} \text{ s}^{-2}$. For the dissipative term, we use the leading-order current-response result for doped graphene [28], $\Im m \chi_{orb}(q, \omega) = \varepsilon_F / (2\pi \hbar^2) \omega / (v_F q)$, from which we identify $\alpha = \varepsilon_F / (2\pi \hbar^2)$. Taking $\varepsilon_F = 0.1 \text{ eV}$, $v_F = 10^6 \text{ m s}^{-1}$, and $c_{ph}/v_F = 10^{-2}$ for monolayer graphene, we obtain $\alpha = 2.29 \times 10^{47} \text{ J}^{-1} \text{ s}^{-2}$. Using the definitions of the rescaled parameters, together with the mass density of a single graphene layer, this gives the effective dimensionless values $\bar{\chi} = 5.3 \times 10^{-9}$ and $\bar{\alpha} = 9.9 \times 10^{-8}$. The small magnitude of these parameters implies that a non-Fermi-liquid regime does not develop at accessible values of $\bar{\varepsilon}$ in monolayer graphene, as seen in Fig. 3.

In contrast, for MATBG the Fermi velocity is strongly reduced. Taking $v_F^* \sim 10^4 \text{ m s}^{-1}$, $\varepsilon_F \sim 1 \text{ meV}$ [29], and $c_{ph}/v_F^* \sim 10^{-1}$ [30], the same procedure yields substantially enhanced effective parameters, $\bar{\chi} = 5.3 \times 10^{-3}$ and $\bar{\alpha} = 0.1$. This enhancement originates from the strong suppression of v_F^* together with the larger low-energy density of states in the moiré bands. Since both the static

coefficient $\bar{\chi}$ and the damping coefficient $\bar{\alpha}$ scale with the electronic response, increasing the density of states enhances both parameters and pushes the crossover scale closer to the Fermi surface. The same mechanism would also operate in monolayer graphene, where increasing the density of states would move the crossover to more accessible fractions of ε_F .

MATBG is particularly interesting because its van Hove singularities lie much closer to charge neutrality than in monolayer graphene [31]. As a result, proximity to the van Hove singularity can make entry into a paramagnetic orbital-response regime plausible, rather than the strongly diamagnetic response more typical of monolayer graphene. In this connection, previous studies have discussed marginal-Fermi-liquid behaviour in MATBG and its competition with other interaction effects [32, 33]. Within the present framework, this makes MATBG a more natural platform for the $\bar{\chi} < 0$ regime discussed in Fig. 2, where the infrared self-energy becomes marginal-Fermi-liquid like. Fig. 3 therefore, highlights a plausible route toward marginal and non-Fermi-liquid behaviour in real materials.

Conclusions—In this work, we studied the electronic self-energy generated by the coupling of electronic currents to gauge phonons. The transverse phonon propagator entering this calculation is itself dressed by the electron-phonon interaction. Since the phonon self-energy is proportional to the transverse current-current response, the resulting low-energy behaviour is controlled by two parameters: the orbital susceptibility χ and the dimensionless damping parameter $\bar{\alpha}$. We showed that when $\bar{\alpha} \gg 1$, *i.e.* when phonons are overdamped, the system exhibits robust non-Fermi-liquid behaviour reminiscent of both quantum-critical metals and systems coupled to transverse gauge fluctuations.

We also found that the sign of χ controls the low-energy structure of the quasiparticle decay rate. For $\chi > 0$, the decay rate remains Fermi-liquid-like only asymptotically close to the Fermi surface and rapidly crosses over to non-Fermi-liquid scaling at higher energies. The corresponding Fermi-liquid window is much narrower than in conventional metals and shrinks with increasing $\bar{\alpha}$. This behaviour resembles that of a system close to, but not exactly at, quantum criticality, where the onset of non-Fermi-liquid behaviour is controlled by the bosonic gap.

More intriguingly, for $\chi < 0$ the Fermi-liquid asymptotic regime is entirely absent. The softened dispersion of the dressed transverse mode instead produces a marginal-Fermi-liquid-like regime at the lowest energies, followed by a crossover to non-Fermi-liquid behaviour at higher energies. The corresponding crossover scale is set by the competition between the bare transverse-phonon dispersion and the orbital-susceptibility correction.

These results identify strain-induced gauge phonons as a novel route to non-Fermi-liquid physics in Dirac materials, with magic-angle twisted bilayer graphene providing a particularly promising platform.

More broadly, the same mechanism may be relevant in systems with different lattice geometries, since the existence of gauge phonons that couple to electronic currents does not rely on hexagonal symmetry alone. Similar gauge-like phonon couplings can arise in other Dirac lattices and may also occur in distorted square-lattice systems where pseudo-gauge fields emerge once lattice symmetry is reduced [21]. In this sense, the present mechanism may offer a complementary microscopic route toward strange-metal phenomenology in a wider class of materials. Assessing its possible relevance to systems such as the cuprates, where linear-in-temperature transport remains a central open problem [4, 5], requires a more detailed investigation that lies beyond the scope of the present work.

Acknowledgments.—AP and AK acknowledge the support of the Leverhulme Trust under Grant Agreement RPG-2023-253. RG acknowledges the support of the Departmental Studentship funded by the Faculty of Science and Engineering, University of Manchester. MP was partly supported by NRRP MUR Project No. PE0000023–NQSTI (Italy) and by the European Union under grant agreement No. 101131579 - Exqiral. Views and opinions expressed in this material are those of the author(s) only and do not necessarily reflect those of the European Union or the European Commission. Neither the European Union nor the granting authority can be held responsible for them.

Appendix A: Derivation of the strain-induced electron–phonon coupling in graphene

In this appendix we derive the low-energy scalar and vector electron–phonon couplings used in Eq. (1), starting from the modulation of nearest-neighbour hoppings by a smooth in-plane displacement field $\mathbf{u}(\mathbf{r})$. In particular, we recover the explicit scalar deformation-potential coupling $V_{\mathbf{q}}$ and the strain-induced gauge field $A_{\mathbf{q},\nu}$ entering the low-energy interaction Hamiltonian. The full low-energy interaction Hamiltonian is

$$\mathcal{H}_{\text{e-ph}} = \sum_{\mathbf{k}, \mathbf{q}, \alpha, \beta} c_{\mathbf{k}-\mathbf{q}, \alpha}^\dagger \left(\mathbf{A}_{\mathbf{q}} \cdot \mathbf{j}_{\mathbf{q}} + V_{\mathbf{q}} \mathbb{1} \right)_{\alpha\beta} c_{\mathbf{k}, \beta}, \quad (\text{A1})$$

where the gauge field couples to the longitudinal and transverse current components $j_{\mathbf{q},L} = v_F \hat{\mathbf{q}} \cdot \boldsymbol{\sigma}$ and $j_{\mathbf{q},T} = v_F (\hat{\mathbf{z}} \times \hat{\mathbf{q}}) \cdot \boldsymbol{\sigma}$, with $\boldsymbol{\sigma} = (\sigma^x, \sigma^y)$. The scalar coupling is

$$V_{\mathbf{q}} = g_1 q \sqrt{\frac{1}{2\rho_m \omega_{\mathbf{q},L}}} \left(a_{\mathbf{q},L} + a_{-\mathbf{q},L}^\dagger \right), \quad (\text{A2})$$

while the gauge-field components take the form

$$A_{\mathbf{q},\nu} = \sum_{\nu'=L,T} g_{\nu'}(q) \tilde{M}_{\nu\nu'}(\hat{\mathbf{q}}) \left(a_{\mathbf{q},\nu'} + a_{-\mathbf{q},\nu'}^\dagger \right), \quad (\text{A3})$$

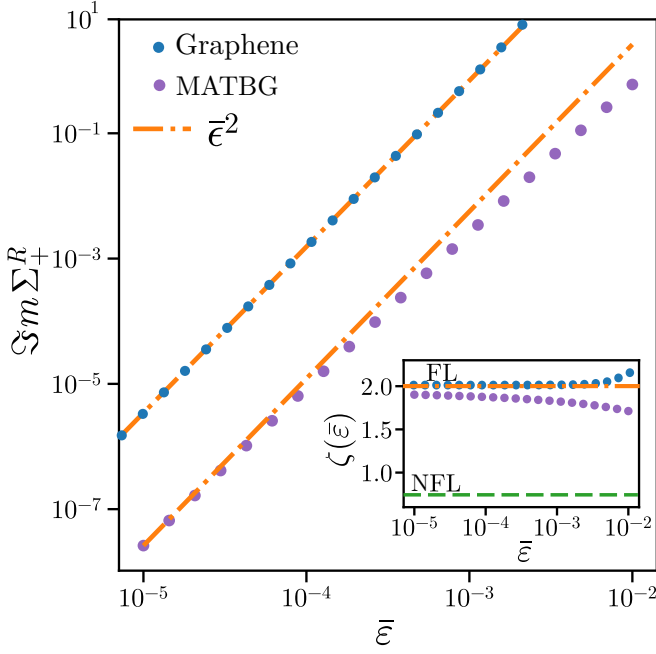


FIG. 3. Imaginary part of the retarded self-energy $\Im m \Sigma_+^R(k_F, \bar{\epsilon})$ for monolayer graphene and MATBG, evaluated using the material parameters discussed in the text. The dashed line shows the Fermi-liquid scaling $\bar{\epsilon}^2$. For monolayer graphene (blue), the self-energy follows the expected Fermi-liquid behaviour over the accessible energy window. In contrast, for MATBG (purple), the enhanced electronic response leads to an observable departure from Fermi-liquid behaviour. The inset shows the local logarithmic slope $\zeta(\bar{\epsilon}) = d \ln \Im m \Sigma_+^R(k_F, \bar{\epsilon}) / d \ln \bar{\epsilon}$, showing $\zeta \rightarrow 2$ for graphene and a steady departure of $\zeta \rightarrow 2$ for MATBG.

with

$$g_\nu(q) = \frac{g_2}{v_F} \sqrt{\frac{q^2}{2\rho_m \omega_{q,\nu}}}, \quad \tilde{M}(\hat{q}) = \begin{pmatrix} \cos \varphi_q & -\sin \varphi_q \\ \sin \varphi_q & \cos \varphi_q \end{pmatrix}. \quad (\text{A4})$$

We now derive these expressions from the strain dependence of the nearest-neighbour hoppings.

Let δ_n ($n = 1, 2, 3$) denote the undeformed nearest-neighbour vectors, with $|\delta_n| = a$ and $\hat{\delta}_n = \delta_n/a$. To linear order in gradients, the deformed bond vectors are

$$\delta'_n(\mathbf{r}) = \delta_n + \mathbf{u}(\mathbf{r} + \delta_n) - \mathbf{u}(\mathbf{r}) \simeq (\mathbb{I} + \nabla \mathbf{u}) \delta_n. \quad (\text{A5})$$

The corresponding fractional bond-length change is

$$\frac{|\delta'_n| - a}{a} \simeq \hat{\delta}_n^T \mathbf{u}(\mathbf{r}) \hat{\delta}_n, \quad u_{ij}(\mathbf{r}) = \frac{1}{2}(\partial_i u_j + \partial_j u_i), \quad (\text{A6})$$

where u_{ij} is the strain tensor.

We model the strain-induced hopping modulation as [22, 34]

$$t_n(\mathbf{r}) = t \exp\left[-\beta \left(\frac{|\delta'_n(\mathbf{r})|}{a} - 1\right)\right] \simeq t + \delta t_n(\mathbf{r}), \quad (\text{A7})$$

which gives, to linear order,

$$\delta t_n(\mathbf{r}) \simeq -\beta t \hat{\delta}_n^T \mathbf{u}(\mathbf{r}) \hat{\delta}_n. \quad (\text{A8})$$

For graphene one has $\beta \simeq 3$ [35].

Near valley \mathbf{K}_τ with $\tau = \pm 1$, we define

$$\delta f_\tau(\mathbf{r}) \equiv \sum_{n=1}^3 \delta t_n(\mathbf{r}) e^{i\mathbf{K}_\tau \cdot \delta_n}. \quad (\text{A9})$$

For the standard nearest-neighbour vectors one finds [34, 35]

$$\delta f_\tau(\mathbf{r}) = \tau \frac{3\beta t}{4} [(u_{xx} - u_{yy}) - i 2u_{xy}]. \quad (\text{A10})$$

This correction enters the Dirac Hamiltonian as a valley-odd pseudo-gauge field. Writing $\Psi_\tau(\mathbf{k})$ for the two-component pseudospin spinor in valley τ , the strain contribution takes the form

$$\mathcal{H}_{\text{strain}} = v_F \sum_{\tau=\pm 1} \sum_{\mathbf{k}, \mathbf{q}} \Psi_\tau^\dagger(\mathbf{k} - \mathbf{q}) [\tau \mathbf{A}(\mathbf{q}) \cdot \boldsymbol{\sigma}] \Psi_\tau(\mathbf{k}), \quad (\text{A11})$$

so that the corresponding current operator is $\mathbf{j} = \delta H / \delta \mathbf{A} = v_F \boldsymbol{\sigma}$. The real-space pseudo-gauge field is therefore

$$\mathbf{A}(\mathbf{r}) = g_2 \begin{pmatrix} u_{xx}(\mathbf{r}) - u_{yy}(\mathbf{r}) \\ -2u_{xy}(\mathbf{r}) \end{pmatrix}, \quad g_2 = \frac{3\beta t}{4}. \quad (\text{A12})$$

We now express $\mathbf{A}(\mathbf{q})$ in terms of phonon modes by quantizing the displacement field as

$$\mathbf{u}(\mathbf{r}) = \frac{1}{\sqrt{N}} \sum_{\mathbf{q}, \nu=L, T} \sqrt{\frac{1}{2\rho_m \omega_{q,\nu}}} \mathbf{e}_\nu(\hat{q}) \times (a_{\mathbf{q},\nu} e^{i\mathbf{q} \cdot \mathbf{r}} + a_{-\mathbf{q},\nu}^\dagger e^{-i\mathbf{q} \cdot \mathbf{r}}), \quad (\text{A13})$$

where $\mathbf{e}_L = \hat{q}$ and $\mathbf{e}_T = \hat{z} \times \hat{q}$. Since $u_{ij}(\mathbf{q}) = \frac{i}{2}(q_i u_j + q_j u_i)$, the combinations entering Eq. (A12) are

$$u_{xx} - u_{yy} = i(q_x u_x - q_y u_y), \quad (\text{A14})$$

$$-2u_{xy} = -i(q_x u_y + q_y u_x). \quad (\text{A15})$$

Writing the displacement in the polarization basis $\mathbf{u} = u_L \hat{q} + u_T (\hat{z} \times \hat{q})$, one has $u_x = \cos \varphi_q u_L - \sin \varphi_q u_T$ and $u_y = \sin \varphi_q u_L + \cos \varphi_q u_T$. Projecting the gauge field onto longitudinal and transverse components, $A_{q,L} = \hat{q} \cdot \mathbf{A}(\mathbf{q})$ and $A_{q,T} = (\hat{z} \times \hat{q}) \cdot \mathbf{A}(\mathbf{q})$, one obtains

$$A_{q,L} = g_2 q (\cos \varphi_q u_L - \sin \varphi_q u_T), \quad (\text{A16})$$

$$A_{q,T} = g_2 q (\sin \varphi_q u_L + \cos \varphi_q u_T). \quad (\text{A17})$$

Here the overall factor of i originating from gradients has been absorbed into the phase convention for the phonon operators, so that $A_{q,\nu}$ is chosen real. Using

$u_\nu(\mathbf{q}) = \sqrt{1/(2\rho_m\omega_{\mathbf{q},\nu})} (a_{\mathbf{q},\nu} + a_{-\mathbf{q},\nu}^\dagger)$, Eq. (A17) reduces to Eq. (A3) with $g_\nu(q)$ and $\tilde{M}(\hat{\mathbf{q}})$ given in Eq. (A4).

Finally, the scalar deformation-potential coupling follows from $V(\mathbf{r}) = g_1(u_{xx} + u_{yy})$. Using Eq. (A13), one finds

$$u_{xx}(\mathbf{q}, \nu) + u_{yy}(\mathbf{q}, \nu) = iq \sqrt{\frac{1}{2\rho_m\omega_{\mathbf{q},\nu}}} (a_{\mathbf{q},\nu} + a_{-\mathbf{q},\nu}^\dagger) (\mathbf{e}_\nu \cdot \hat{\mathbf{q}}), \quad (\text{A18})$$

so that only longitudinal phonons contribute. This yields Eq. (A2),

$$V_{\mathbf{q}} = g_1 q \sqrt{\frac{1}{2\rho_m\omega_{\mathbf{q},L}}} (a_{\mathbf{q},L} + a_{-\mathbf{q},L}^\dagger). \quad (\text{A19})$$

For completeness, the explicit gauge-field coupling entering the main text is therefore

$$A_{\mathbf{q},\nu} = \sum_{\nu'=L,T} g_{\nu'}(q) \tilde{M}_{\nu\nu'}(\hat{\mathbf{q}}) (a_{\mathbf{q},\nu'} + a_{-\mathbf{q},\nu'}^\dagger), \quad (\text{A20})$$

with

$$g_\nu(q) = \frac{g_2}{v_F} \sqrt{\frac{q^2}{2\rho_m\omega_{\mathbf{q},\nu}}}, \quad \tilde{M}(\hat{\mathbf{q}}) = \begin{pmatrix} \cos \varphi_{\mathbf{q}} & -\sin \varphi_{\mathbf{q}} \\ \sin \varphi_{\mathbf{q}} & \cos \varphi_{\mathbf{q}} \end{pmatrix}. \quad (\text{A21})$$

Appendix B: Self-energy derivation

In this appendix we provide the intermediate steps leading from the Matsubara Fock self-energy, Eq. (2), to the real-frequency expression Eq. (3) and to the transverse-only form used in the low-energy analysis.

We begin by recalling the dressed phonon propagator as the Matsubara correlator of the vector-potential components,

$$D^{\nu\nu'}(\mathbf{q}, i\omega_m) = \int_0^\beta d\tau e^{i\omega_m\tau} \langle \mathcal{T}_\tau A_{\mathbf{q},\nu}(\tau) A_{-\mathbf{q},\nu'}(0) \rangle. \quad (\text{B1})$$

The bare electron Green's function is

$$G_\lambda^{(0)}(\mathbf{k}, i\varepsilon_n) = \frac{1}{i\varepsilon_n - \xi_{\mathbf{k},\lambda}}. \quad (\text{B2})$$

For later use, the Cartesian current matrix elements between incoming and outgoing Dirac states are

$$j_{\mathbf{k},\lambda;\mathbf{k}',\lambda'}^x = v_F \frac{\lambda e^{-i\varphi_{\mathbf{k}}} + \lambda' e^{i\varphi_{\mathbf{k}'}}}{2}, \quad (\text{B3})$$

$$j_{\mathbf{k},\lambda;\mathbf{k}',\lambda'}^y = v_F \frac{i\lambda e^{-i\varphi_{\mathbf{k}}} - i\lambda' e^{i\varphi_{\mathbf{k}'}}}{2}. \quad (\text{B4})$$

Since we need the retarded self-energy, we analytically continue $i\varepsilon_n \rightarrow \varepsilon + i0^+$. Starting from Eq. (2), we rewrite

the Matsubara sum as a contour integral,

$$\begin{aligned} \Sigma_\lambda(\mathbf{k}, i\varepsilon_n) &= - \oint \frac{dz}{2\pi i} n_B(z) \sum_{\nu,\nu',\lambda'} \int \frac{d^2\mathbf{q}}{(2\pi)^2} \\ &\times j_{\mathbf{k},\lambda;\mathbf{k}+\mathbf{q},\lambda'}^\nu j_{\mathbf{k}+\mathbf{q},\lambda';\mathbf{k},\lambda}^{\nu'} D^{\nu,\nu'}(\mathbf{q}, z) G_{\lambda'}^{(0)}(\mathbf{k} + \mathbf{q}, i\varepsilon_n + z). \end{aligned} \quad (\text{B5})$$

Here D and $G^{(0)}$ are understood as the bosonic and fermionic propagators analytically continued away from the Matsubara axis. The integrand has branch cuts at $\Im m(z) = 0$ and $\Im m(z) = -i\varepsilon_n$. Integrating along these branch cuts and continuing $i\varepsilon_n \rightarrow \varepsilon + i0^+$ yields

$$\begin{aligned} \Sigma_\lambda^{(R)}(\mathbf{k}, \varepsilon) &= - \int_{-\infty}^{\infty} \frac{d\omega}{\pi} \sum_{\nu,\nu',\lambda'} \int \frac{d^2\mathbf{q}}{(2\pi)^2} j_{\mathbf{k},\lambda;\mathbf{k}+\mathbf{q},\lambda'}^\nu j_{\mathbf{k}+\mathbf{q},\lambda';\mathbf{k},\lambda}^{\nu'} \\ &\times \left[n_B(\omega) \Im m D^{\nu,\nu'}(\mathbf{q}, \omega + i\eta) G_{\lambda'}^{(0)}(\mathbf{k} + \mathbf{q}, \varepsilon + \omega + i\eta) \right. \\ &\left. - n_F(\omega + \varepsilon) D^{\nu,\nu'}(\mathbf{q}, \omega - i\eta) \Im m G_{\lambda'}^{(0)}(\mathbf{k} + \mathbf{q}, \varepsilon + \omega + i\eta) \right], \end{aligned} \quad (\text{B6})$$

with $\eta \rightarrow 0^+$. Taking the imaginary part gives

$$\begin{aligned} \Im m \Sigma_\lambda^R(\mathbf{k}, \varepsilon) &= - \int_{-\infty}^{\infty} \frac{d\omega}{\pi} [n_B(\omega) + n_F(\omega + \varepsilon)] \\ &\times \sum_{\nu,\nu',\lambda'} \int \frac{d^2\mathbf{q}}{(2\pi)^2} \Im m D^{\nu\nu'}(\mathbf{q}, \omega) \Im m G_{\lambda'}^{(0)}(\mathbf{k} + \mathbf{q}, \varepsilon + \omega) \\ &\times j_{\mathbf{k},\lambda;\mathbf{k}+\mathbf{q},\lambda'}^\nu j_{\mathbf{k}+\mathbf{q},\lambda';\mathbf{k},\lambda}^{\nu'}, \end{aligned} \quad (\text{B7})$$

which is Eq. (3) of the main text.

We now take the low-energy limit at the Fermi surface. Evaluating the bare retarded Green's function, $G_{\lambda'}^{R,(0)}(\mathbf{p}, \varepsilon) = 1/(\varepsilon - \xi_{\mathbf{p},\lambda'} + i0^+)$, gives

$$\Im m G_{\lambda'}^{R,(0)}(\mathbf{k} + \mathbf{q}, \varepsilon + \omega) = -\pi \delta(\varepsilon + \omega - \xi_{\mathbf{k}+\mathbf{q},\lambda'}), \quad (\text{B8})$$

which pins the intermediate fermionic state to the mass shell $\xi_{\mathbf{k}+\mathbf{q},\lambda'} = \varepsilon + \omega$.

In the $T \rightarrow 0$ limit, the thermal factor in Eq. (B7) simplifies to

$$n_B(\omega) + n_F(\omega + \varepsilon) = -\Theta(-\omega) + \Theta(-\omega - \varepsilon). \quad (\text{B9})$$

For $\varepsilon > 0$, this equals -1 for $\omega \in (-\varepsilon, 0)$ and vanishes otherwise, while for $\varepsilon < 0$ it equals $+1$ for $\omega \in (0, -\varepsilon)$. This yields the compact frequency window $\omega \in [\min(0, -\varepsilon), \max(0, -\varepsilon)]$.

Finally, for $\mathbf{k} \simeq \mathbf{k}_F$, the on-shell condition in Eq. (B8) implies that $\mathbf{k}' = \mathbf{k} + \mathbf{q}$ also lies close to the Fermi surface. In this limit, the longitudinal and transverse current matrix elements can be constructed from Eq. (B4) as

$$j_{\mathbf{k},\lambda;\mathbf{k}',\lambda'}^L = \hat{\mathbf{q}} \cdot \mathbf{j}_{\mathbf{k},\lambda;\mathbf{k}',\lambda'} = v_F \frac{i(\lambda' - \lambda)}{2} e^{i(\varphi_{\mathbf{k}'} - \varphi_{\mathbf{k}})/2}, \quad (\text{B10})$$

$$j_{\mathbf{k},\lambda;\mathbf{k}',\lambda'}^T = (\hat{\mathbf{z}} \times \hat{\mathbf{q}}) \cdot \mathbf{j}_{\mathbf{k},\lambda;\mathbf{k}',\lambda'} = v_F \frac{\lambda' + \lambda}{2} e^{i(\varphi_{\mathbf{k}'} - \varphi_{\mathbf{k}})/2}. \quad (\text{B11})$$

At the Fermi surface one has $\lambda' = \lambda$, so the longitudinal matrix element vanishes and only the transverse channel survives. Equation (B7) therefore reduces to

$$\begin{aligned} \Im m \Sigma_+^{(R)}(\mathbf{k}, \varepsilon) &= -v_F^2 \int_{\min(0, -\varepsilon)}^{\max(0, -\varepsilon)} \frac{d\omega}{\pi} \int \frac{d^2 \mathbf{q}}{(2\pi)^2} \\ &\times \Im m D^{TT}(\mathbf{q}, \omega) \Im m G_+^{(0)}(\mathbf{k} + \mathbf{q}, \varepsilon + \omega), \end{aligned} \quad (\text{B12})$$

which is the transverse-only form used in the main text.

Appendix C: Bare and RPA-dressed transverse phonon propagator

In this appendix we summarize the intermediate steps entering the dressed transverse phonon propagator and the dimensionless self-energy used in the main text. We first derive the bare transverse–transverse (TT) propagator from the gauge-field coupling, then discuss its RPA-like dressing in the transverse current channel, and finally show the angular integration used to obtain the reduced self-energy.

The gauge-field components are linear combinations of phonon coordinates, as seen in Eq. A21. The bosonic propagator is canonically defined as

$$D^{\nu\nu'}(\mathbf{q}, i\omega_m) = \int_0^\beta d\tau e^{i\omega_m \tau} \langle \mathcal{T}_\tau A_{\mathbf{q}, \nu}(\tau) A_{-\mathbf{q}, \nu'}(0) \rangle. \quad (\text{C1})$$

Using the free-phonon correlator

$$\begin{aligned} &\int_0^\beta d\tau e^{i\omega_m \tau} \left\langle \mathcal{T}_\tau (a_{\mathbf{q}, \nu}(\tau) + a_{-\mathbf{q}, \nu}^\dagger(\tau)) \right. \\ &\times \left. (a_{-\mathbf{q}, \nu}(0) + a_{\mathbf{q}, \nu}^\dagger(0)) \right\rangle = \frac{2\omega_{\mathbf{q}, \nu}}{(i\omega_m)^2 - \omega_{\mathbf{q}, \nu}^2}, \end{aligned} \quad (\text{C2})$$

and one finds for the bare TT component

$$\begin{aligned} D^{(0), TT}(\mathbf{q}, i\omega_m) &= \sum_{\nu=L, T} g_\nu^2(q) \\ &\times [\tilde{M}_{T, \nu}(\hat{\mathbf{q}})]^2 \frac{2\omega_{\mathbf{q}, \nu}}{(i\omega_m)^2 - \omega_{\mathbf{q}, \nu}^2}. \end{aligned} \quad (\text{C3})$$

We now show the angular integration used after inserting the dressed propagator into the low-energy self-energy. Defining

$$\begin{aligned} \mathcal{I}(k, q, \varepsilon + \omega + \mu) &\equiv \int_0^{2\pi} \frac{d\varphi_{\mathbf{q}}}{2\pi} \Im m G_+^{(0)}(\mathbf{k} + \mathbf{q}, \varepsilon + \omega + i0^+) \\ &= - \int_0^\pi d\varphi_{\mathbf{q}} \delta(\varepsilon + \omega + \mu - v_F |\mathbf{k} + \mathbf{q}|), \end{aligned} \quad (\text{C4})$$

the delta function implies $\varepsilon + \omega + \mu > 0$ and, choosing $\varphi_{\mathbf{k}} = 0$,

$$\cos \varphi_{\mathbf{q}} = \frac{(\varepsilon + \omega + \mu)^2 - v_F^2(k^2 + q^2)}{2v_F^2 k q}. \quad (\text{C5})$$

The condition $-1 \leq \cos \varphi_{\mathbf{q}} \leq 1$ restricts the momentum integration to $q_{\min} < q < q_{\max}$, with

$$\begin{aligned} v_F q_{\min} &= \max\left(0, v_F k - \mu - \varepsilon - \omega, \varepsilon + \omega + \mu - v_F k\right), \\ v_F q_{\max} &= \varepsilon + \omega + \mu + v_F k. \end{aligned} \quad (\text{C6})$$

Under these conditions,

$$\begin{aligned} \mathcal{I}(k, q, \varepsilon + \omega + \mu) &= -2 |\varepsilon + \omega + \mu| \\ &\times \left[(2v_F^2 k q)^2 - ((\varepsilon + \omega + \mu)^2 - v_F^2(k^2 + q^2))^2 \right]^{-1/2}. \end{aligned} \quad (\text{C7})$$

Substituting this result into the low-energy self-energy and then rescaling to dimensionless variables leads to Eq. (10) in the main text.

Appendix D: Power laws of the self-energy

In this appendix we extract the low-energy power laws of the imaginary part of the retarded self-energy at the Fermi surface from the low-energy form of the dressed TT phonon propagator. Throughout we set $\mathbf{k} \simeq \mathbf{k}_F$ and consider $0 < \varepsilon \ll \mu$, so that at $T = 0$ the frequency transfer is restricted to $\omega \in [-\varepsilon, 0]$. It is convenient to write the self-energy in the schematic form

$$\begin{aligned} \Im m \Sigma_+^R(k_F, \varepsilon) &\simeq -C \int_{-\varepsilon}^0 \frac{d\omega}{\pi} \int_{q_{\min}}^{q_{\max}} \frac{dq}{\pi} \mathcal{K}(q, \omega, \varepsilon) \\ &\times \frac{\bar{\alpha} q^3 |\omega|}{[\omega^2 - (c_{\text{ph}}/v_F)^2 q^2 - \bar{\chi} q^4]^2 + \bar{\alpha}^2 q^2 \omega^2}, \end{aligned} \quad (\text{D1})$$

where $C = g_2^2/\rho_m$ absorbs smooth prefactors, and \mathcal{K} denotes the kinematic factor in Eq. C7. For $\mathbf{k} \simeq \mathbf{k}_F$ this factor is smooth and finite away from the integration endpoints. At the endpoints, \mathcal{K} has a singularity, which is integrable using the Duffy coordinate transformation. Thus, the scaling is governed by the bosonic kernel.

It is useful to keep in mind that the frequency integral is dominated by $|\omega| \sim \varepsilon$. The scaling of the self-energy is therefore determined by the characteristic momenta selected by the peak of the bosonic factor. In the large $\bar{\alpha}$ regime the dressed phonon is overdamped, and this is precisely the regime in which anomalous scaling emerges. However, overdamping alone does not guarantee non-Fermi-liquid behaviour, depending on which momentum region dominates the integral, the self-energy may still remain Fermi-liquid-like.

1. Overdamped reduction for large $\bar{\alpha}$

When $\bar{\alpha}$ is large, the characteristic momenta selected by the bosonic kernel satisfy $q \gg |\omega|$ in the regimes of

interest. One may then neglect the ω^2 term inside the square brackets of Eq. (D1), so that

$$\begin{aligned} & [\omega^2 - (c_{\text{ph}}/v_{\text{F}})^2 q^2 - \bar{\chi} q^4]^2 + \bar{\alpha}^2 q^2 \omega^2 \\ & \simeq q^2 \left[(c_{\text{ph}}/v_{\text{F}})^2 + \bar{\chi} q^2 \right]^2 + \bar{\alpha}^2 \omega^2. \end{aligned} \quad (\text{D2})$$

The bosonic factor then reduces to

$$\begin{aligned} & \frac{\bar{\alpha} q^3 |\omega|}{[\omega^2 - (c_{\text{ph}}/v_{\text{F}})^2 q^2 - \bar{\chi} q^4]^2 + \bar{\alpha}^2 q^2 \omega^2} \\ & \simeq \frac{\bar{\alpha} q |\omega|}{q^2 [(c_{\text{ph}}/v_{\text{F}})^2 + \bar{\chi} q^2]^2 + \bar{\alpha}^2 \omega^2}. \end{aligned} \quad (\text{D3})$$

The scaling of the self-energy is therefore controlled by the momenta at which the denominator of Eq. (D3) is minimal.

2. Fermi-liquid-like regime for $\bar{\chi} > 0$

We first consider the regime in which the quartic term is negligible, *i.e.* when $\bar{\chi} q^2 \ll (c_{\text{ph}}/v_{\text{F}})^2$. In this case the denominator of Eq. (D3) reduces to

$$(c_{\text{ph}}/v_{\text{F}})^4 q^2 + \bar{\alpha}^2 \omega^2, \quad (\text{D4})$$

so the integrand is peaked at

$$q_{\text{FL}} \sim \frac{\bar{\alpha}}{(c_{\text{ph}}/v_{\text{F}})^2} |\omega|. \quad (\text{D5})$$

Since the frequency integral is restricted to $|\omega| \lesssim \varepsilon$, the dominant contribution comes from $|\omega| \sim \varepsilon$, giving

$$q_{\text{FL}} \sim \frac{\bar{\alpha}}{(c_{\text{ph}}/v_{\text{F}})^2} \varepsilon. \quad (\text{D6})$$

Thus q scales linearly with ε . We may then set $\omega = \bar{\omega} \varepsilon$ and $q = \bar{q} \varepsilon$ in Eq. (D1). Since the measure contributes $d\omega dq \sim \varepsilon^2$, while both \mathcal{K} and the overdamped kernel remain finite in this scaling limit, one obtains

$$\begin{aligned} \Im m \Sigma_+^{(R)}(k_{\text{F}}, \varepsilon) & \simeq -\frac{g_2^2}{\rho_m} \int_{-1}^0 \frac{d\bar{\omega}}{\pi} \varepsilon \int_{1+\bar{\omega}}^{2v_{\text{F}}k_{\text{F}}/\varepsilon + (1+\bar{\omega})} \frac{d\bar{q}}{\pi} \varepsilon \\ & \times \frac{\varepsilon^2 \bar{q} |1 + \bar{\omega} + \varepsilon_{\text{F}}/\varepsilon|}{\varepsilon^2 \sqrt{4\varepsilon_{\text{F}}^2 \bar{q}^2/\varepsilon^2 - \left[(1 + \bar{\omega} + \varepsilon_{\text{F}}/\varepsilon)^2 - \varepsilon_{\text{F}}^2/\varepsilon^2 - \bar{q}^2 \right]^2}} \\ & \times \frac{\varepsilon^2 \alpha \bar{q} \bar{\omega}}{\varepsilon^2 \left((c_{\text{ph}}/v_{\text{F}})^4 \bar{q}^2 + \bar{\alpha}^2 \bar{\omega}^2 \right)} \\ & \rightarrow -\varepsilon^2 \frac{g_2^2}{\rho_m} \int_{-1}^0 \frac{d\bar{\omega}}{\pi} \int_{1+\bar{\omega}}^{\infty} \frac{d\bar{q}}{\pi} \\ & \times \frac{\bar{q}}{2\sqrt{\bar{q}^2 - (1 + \bar{\omega})^2}} \frac{\bar{\alpha} \bar{q} \bar{\omega}}{(c_{\text{ph}}/v_{\text{F}})^4 \bar{q}^2 + \bar{\alpha}^2 \bar{\omega}^2}. \end{aligned} \quad (\text{D7})$$

Hence the self-energy remains Fermi-liquid like, even though the phonon mode is overdamped.

3. Non-Fermi-liquid regime for $\bar{\chi} > 0$

We now consider the regime in which the quartic term dominates over the acoustic piece,

$$(c_{\text{ph}}/v_{\text{F}})^2 \ll \bar{\chi} q^2. \quad (\text{D8})$$

Then the q -dependent part of the denominator in Eq. (D3) becomes $\sim \bar{\chi}^2 q^6$, and the bosonic kernel is peaked at

$$q_{\text{NFL}} \sim \left(\frac{\bar{\alpha} |\omega|}{\bar{\chi}} \right)^{1/3}. \quad (\text{D9})$$

Again taking $|\omega| \sim \varepsilon$, this gives

$$q_{\text{NFL}} \sim \left(\frac{\bar{\alpha} \varepsilon}{\bar{\chi}} \right)^{1/3}. \quad (\text{D10})$$

In this regime $q_{\text{NFL}} \gg |\omega|$ parametrically as $\varepsilon \rightarrow 0$, so the overdamped approximation is self-consistent. We now scale

$$\omega = \bar{\omega} \varepsilon, \quad q = \bar{q} \left(\frac{\bar{\alpha} \varepsilon}{\bar{\chi}} \right)^{1/3}. \quad (\text{D11})$$

Then Eq. (D1)

$$\begin{aligned} \Im m \Sigma_+^{(R)}(k_{\text{F}}, \varepsilon) & \rightarrow -\varepsilon^{2/3} \frac{g_2^2}{\rho_m} \int_{-1}^0 \frac{d\bar{\omega}}{\pi} \int_0^{\infty} \frac{d\bar{q}}{2\pi} \\ & \times \frac{\bar{\alpha} \bar{q} \bar{\omega}}{\bar{\chi}^2 \bar{q}^6 + \bar{\alpha}^2 \bar{\omega}^2}. \end{aligned} \quad (\text{D12})$$

The remaining integral is finite, so that

$$\Im m \Sigma_+^{(R)}(k_{\text{F}}, \varepsilon) \propto \varepsilon^{2/3}. \quad (\text{D13})$$

4. Crossover scale for $\bar{\chi} > 0$

The crossover between the Fermi-liquid like and non-Fermi-liquid regimes occurs when the characteristic momenta Eqs. (D5) and (D9) become comparable:

$$\frac{\bar{\alpha}}{(c_{\text{ph}}/v_{\text{F}})^2} \varepsilon \sim \left(\frac{\bar{\alpha} \varepsilon}{\bar{\chi}} \right)^{1/3}. \quad (\text{D14})$$

Solving for ε gives

$$\varepsilon_* \sim \frac{(c_{\text{ph}}/v_{\text{F}})^3}{\bar{\alpha} \sqrt{\bar{\chi}}}. \quad (\text{D15})$$

For $\varepsilon \ll \varepsilon_*$ the self-energy is Fermi-liquid like, Eq. (D7), whereas for $\varepsilon \gg \varepsilon_*$ it crosses over to the non-Fermi-liquid form Eq. (D13).

5. Soft-shell scaling for $\bar{\chi} < 0$

We now consider the case $\bar{\chi} < 0$. Writing $\bar{\chi} = -|\bar{\chi}|$, the real part of the bosonic denominator softens at the finite momentum

$$q_{\text{shell}} = \frac{(c_{\text{ph}}/v_{\text{F}})}{\sqrt{|\bar{\chi}|}}. \quad (\text{D16})$$

This is the soft shell discussed in the main text.

In the overdamped limit, the bosonic denominator becomes

$$q^2 \left[(c_{\text{ph}}/v_{\text{F}})^2 - |\bar{\chi}|q^2 \right]^2 + \bar{\alpha}^2 \omega^2, \quad (\text{D17})$$

which is minimized near $q = q_{\text{shell}}$. We therefore write

$$q = q_{\text{shell}} + \delta q, \quad |\delta q| \ll q_{\text{shell}}. \quad (\text{D18})$$

Expanding the real part of the denominator around q_{shell} gives

$$\begin{aligned} (c_{\text{ph}}/v_{\text{F}})^2 - |\bar{\chi}|q^2 &= (c_{\text{ph}}/v_{\text{F}})^2 - |\bar{\chi}|(q_{\text{shell}} + \delta q)^2 \\ &\simeq -2|\bar{\chi}|q_{\text{shell}} \delta q, \end{aligned} \quad (\text{D19})$$

since $(c_{\text{ph}}/v_{\text{F}})^2 - |\bar{\chi}|q_{\text{shell}}^2 = 0$ by definition of q_{shell} . Substituting this into the denominator yields

$$\begin{aligned} q^2 \left[(c_{\text{ph}}/v_{\text{F}})^2 - |\bar{\chi}|q^2 \right]^2 + \bar{\alpha}^2 \omega^2 \\ \simeq 4|\bar{\chi}|^2 q_{\text{shell}}^4 (\delta q)^2 + \bar{\alpha}^2 \omega^2. \end{aligned} \quad (\text{D20})$$

Thus, close to the shell, the bosonic factor takes a Lorentzian form in δq ,

$$\frac{\bar{\alpha}q|\omega|}{q^2 \left[(c_{\text{ph}}/v_{\text{F}})^2 - |\bar{\chi}|q^2 \right]^2 + \bar{\alpha}^2 \omega^2} \simeq \frac{\bar{\alpha}q_{\text{shell}}|\omega|}{4|\bar{\chi}|^2 q_{\text{shell}}^4 (\delta q)^2 + \bar{\alpha}^2 \omega^2}. \quad (\text{D21})$$

The apparent singularity at $q = q_{\text{shell}}$ is therefore regulated by the damping term and does not produce a divergence.

Balancing the two terms in Eq. (D20) gives the shell width

$$\delta q_{\text{shell}} \sim \frac{\alpha}{2|\bar{\chi}|q_{\text{shell}}^2} |\omega| = \frac{\alpha}{2(c_{\text{ph}}/v_{\text{F}})^2} |\omega|. \quad (\text{D22})$$

Since the remaining kinematic factors are smooth at finite momentum $q \simeq q_{\text{shell}}$, the singular part of the q integral reduces to

$$I_{\text{shell}}(\omega) \sim \int_{q_{\text{min}} - q_{\text{shell}}}^{q_{\text{max}} - q_{\text{shell}}} d(\delta q) \frac{\bar{\alpha}q_{\text{shell}}|\omega|}{4|\bar{\chi}|^2 q_{\text{shell}}^4 (\delta q)^2 + \bar{\alpha}^2 \omega^2}, \quad (\text{D23})$$

where

$$q_{\text{min}} = \frac{\varepsilon + \omega}{v_{\text{F}}}, \quad q_{\text{max}} = 2k_{\text{F}} + \frac{\varepsilon + \omega}{v_{\text{F}}}. \quad (\text{D24})$$

We now rescale

$$\delta q = |\omega|x, \quad d(\delta q) = |\omega|dx. \quad (\text{D25})$$

Then Eq. (D23) becomes

$$\begin{aligned} I_{\text{shell}}(\omega) &\sim \int_{x_{\text{min}}}^{x_{\text{max}}} |\omega| dx \frac{\bar{\alpha}q_{\text{shell}}|\omega|}{4|\bar{\chi}|^2 q_{\text{shell}}^4 \omega^2 x^2 + \bar{\alpha}^2 \omega^2} \\ &\sim \int_{x_{\text{min}}}^{x_{\text{max}}} dx \frac{\bar{\alpha}q_{\text{shell}}}{4|\bar{\chi}|^2 q_{\text{shell}}^4 x^2 + \bar{\alpha}^2}, \end{aligned} \quad (\text{D26})$$

with

$$x_{\text{min}} = \frac{q_{\text{min}} - q_{\text{shell}}}{|\omega|}, \quad x_{\text{max}} = \frac{q_{\text{max}} - q_{\text{shell}}}{|\omega|}. \quad (\text{D27})$$

If the shell lies well inside the allowed integration region, *i.e.*, $q_{\text{min}} \ll q_{\text{shell}} \ll q_{\text{max}}$, then in the low-energy limit $|\omega| \rightarrow 0$ one has

$$x_{\text{min}} \rightarrow -\infty, \quad x_{\text{max}} \rightarrow +\infty. \quad (\text{D28})$$

Therefore the shell contribution reduces to the full-line Lorentzian integral

$$I_{\text{shell}}(\omega) \sim \int_{-\infty}^{+\infty} dx \frac{\bar{\alpha}q_{\text{shell}}}{4|\bar{\chi}|^2 q_{\text{shell}}^4 x^2 + \bar{\alpha}^2}, \quad (\text{D29})$$

which is independent of ω up to a finite dimensionless constant. Hence

$$I_{\text{shell}}(\omega) \sim \omega^0. \quad (\text{D30})$$

Since the ω integral extends over a window of width ε , the soft-shell contribution to the self-energy scales as

$$\Im m \Sigma_+^{(R)}(k_{\text{F}}, \varepsilon) \propto \varepsilon. \quad (\text{D31})$$

Hence the $\bar{\chi} < 0$ regime yields a marginal-Fermi-liquid like contribution dominated by the soft shell. At higher energies the large- q part of the overdamped kernel can again take over, leading to the same crossover scale as in the $\bar{\chi} > 0$ case. Equating the soft-shell momentum q_{shell} with the non-Fermi-liquid momentum scale gives $\frac{(c_{\text{ph}}/v_{\text{F}})}{\sqrt{|\bar{\chi}|}} \sim ((\alpha\varepsilon)/|\bar{\chi}|)^{1/3}$, and therefore $\varepsilon_* \sim (c_{\text{ph}}/v_{\text{F}})^3 / (\bar{\alpha}\sqrt{|\bar{\chi}|})$.

Thus the $\bar{\chi} < 0$ regime exhibits a marginal-Fermi-liquid like infrared behaviour, followed by a crossover into the same non-Fermi-liquid regime encountered for $\bar{\chi} > 0$.

-
- [1] A. A. Abrikosov, L. P. Gorkov, and I. E. Dzyaloshinskii, *Methods of Quantum Field Theory in Statistical Physics* (Dover Publications, New York, 1975) original Russian edition (1962).
- [2] L. D. Landau, Soviet Physics JETP **3**, 920 (1957), zh. Eksp. Teor. Fiz. 30, 1058 (1956).
- [3] L. D. Landau, Soviet Physics JETP **5**, 101 (1957), zh. Eksp. Teor. Fiz. 32, 59 (1957).
- [4] J. A. N. Bruin, H. Sakai, R. S. Perry, and A. P. Mackenzie, *Science* **339**, 804 (2013).
- [5] A. Legros, S. Benhabib, W. Tabiś, F. Laliberté, M. Dion, M. Lizaire, B. Vignolle, D. Vignolles, H. Raffy, Z. Z. Li, P. Auban-Senzier, N. Doiron-Leyraud, P. Fournier, D. Colson, L. Taillefer, and C. Proust, *Nature Physics* **15**, 142 (2019).
- [6] C. M. Varma, P. B. Littlewood, S. Schmitt-Rink, E. Abrahams, and A. E. Ruckenstein, *Physical Review Letters* **63**, 1996 (1989).
- [7] J. A. Hertz, *Physical Review B* **14**, 1165 (1976).
- [8] A. J. Millis, *Physical Review B* **48**, 7183 (1993).
- [9] H. von Löhneysen, A. Rosch, M. Vojta, and P. Wölfle, *Reviews of Modern Physics* **79**, 1015 (2007).
- [10] A. Abanov, A. V. Chubukov, and J. Schmalian, *Advances in Physics* **52**, 119 (2003).
- [11] M. A. Metlitski and S. Sachdev, *Phys. Rev. B* **82**, 075127 (2010).
- [12] D. F. Mross, J. McGreevy, H. Liu, and T. Senthil, *Phys. Rev. B* **82**, 045121 (2010).
- [13] A. A. Patel, H. Guo, I. Esterlis, and S. Sachdev, *Science* **381**, 790 (2023).
- [14] J. Polchinski, *Nuclear Physics B* **422**, 617 (1994).
- [15] B. L. Altshuler, L. B. Ioffe, and A. J. Millis, *Physical Review B* **50**, 14048 (1994).
- [16] S.-S. Lee, *Physical Review B* **80**, 165102 (2009).
- [17] P. A. Lee, N. Nagaosa, and X.-G. Wen, *Reviews of Modern Physics* **78**, 17 (2006).
- [18] P. Rao and F. Piazza, *Physical Review Letters* **130**, 083603 (2023).
- [19] V. Rokaj, M. Ruggenthaler, F. G. Eich, and A. Rubio, *Physical Review Research* **2**, 013012 (2020).
- [20] T. Sohler, M. Calandra, C.-H. Park, N. Bonini, N. Marzari, and F. Mauri, *Physical Review B* **90**, 125414 (2014).
- [21] J. Sun, X. Zhu, T. Liu, S. Feng, and H. Guo, *Physical Review B* **108**, 205149 (2023).
- [22] M. A. H. Vozmediano, M. I. Katsnelson, and F. Guinea, *Physics Reports* **496**, 109 (2010).
- [23] F. Guinea, M. I. Katsnelson, and A. K. Geim, *Nature Physics* **6**, 30 (2010).
- [24] K. Kaasbjerg, K. S. Thygesen, and K. W. Jacobsen, *Physical Review B—Condensed Matter and Materials Physics* **85**, 165440 (2012).
- [25] D. Guerci, P. Simon, and C. Mora, *Physical Review Letters* **125**, 257604 (2020).
- [26] S. A. Brazovskii, *Sov. Phys. JETP* **41**, 85 (1975).
- [27] G. Gómez-Santos and T. Stauber, *Physical review letters* **106**, 045504 (2011).
- [28] A. Principi, M. Polini, and G. Vignale, *Physical Review B—Condensed Matter and Materials Physics* **80**, 075418 (2009).
- [29] E. S. Morell, J. Correa, P. Vargas, M. Pacheco, and Z. Barticevic, *Physical Review B* **82**, 121407 (2010).
- [30] F. Wu, E. Hwang, and S. D. Sarma, *arXiv* (2018), theoretical resistivity study showing suppression of renormalized Fermi velocity in TBG near magic angle.
- [31] R. Bistritzer and A. H. MacDonald, *Proceedings of the National Academy of Sciences* **108**, 12233 (2011).
- [32] J. González and T. Stauber, *Phys. Rev. Lett.* **124**, 186801 (2020).
- [33] Y. Cao et al., *Phys. Rev. Lett.* **124**, 076801 (2020).
- [34] F. de Juan, M. Sturla, and M. A. Vozmediano, *Physical review letters* **108**, 227205 (2012).
- [35] M. A. H. Vozmediano, *Philosophical Transactions: Mathematical, Physical and Engineering Sciences* **369**, 2625 (2011).